

Advantage of U + U over Au + Au collisions at the Relativistic Heavy Ion Collider

C. Nepali, G. Fai, and D. Keane
Center for Nuclear Research, Department of Physics
Kent State University, Kent, OH 44242, USA
(Dated: February 8, 2020)

Collisions of deformed uranium nuclei are studied in a Monte-Carlo Glauber model. For U + U at zero impact parameter ($b = 0$) in the most favorable orientation (tip-to-tip), the transverse particle density (charged-particle rapidity density per weighted transverse area of the initial participant zone) increases by about 35% compared to Au + Au at $b = 0$. To estimate the advantage of U + U over Au + Au in the context of real experiments at the Relativistic Heavy Ion Collider, we examine the effect of a range of centrality cuts on the event sample. In terms of the transverse particle density, the predicted advantage of U + U is about 16%.

PACS numbers: 25.75.-q, 25.75.Ld, 24.85.+p

I. INTRODUCTION

Large space-time volumes with the highest energy density to date, over $15 \text{ GeV}/\text{fm}^3$ in typical estimates [1], have been produced in $\sqrt{s_{NN}} = 200 \text{ GeV}$ Au + Au collisions at the Relativistic Heavy Ion Collider (RHIC) [2, 3, 4, 5]. At such high energy densities, strongly interacting matter is predicted to be in a phase commonly referred to as quark-gluon plasma (QGP) [6]. A goal of the RHIC program is to study this phase in the extended systems created in relativistic collisions of heavy nuclei.

The presence of QGP manifests itself in the equation of state, which (together with the initial conditions) determines various measured properties and serves as an input to fluid-dynamical calculations. It is reasonable to expect that, barring calculational problems, the main features of the equation of state can be probed by comparing fluid-dynamically calculated quantities to data. It has been argued recently that the quark-gluon matter produced in 200 GeV central Au + Au collisions behaves as a perfect fluid with negligible viscosity [7, 8]. This conclusion was based in part on the agreement [5] of the flow quantity $v_2 = \langle \cos(2\phi) \rangle$ (see Eqs. (1) and (2) for a definition) in central Au + Au with the prediction of an ideal-fluid calculation [9]. The data seem to indicate that the system produced in 200 GeV central Au + Au collisions have just reached a large enough energy density in a sufficient space-time volume for the approximate agreement with the fluid-dynamical results. If energy density could be increased even further, a crucial test would be whether $v_2 = \langle \cos(2\phi) \rangle$ continues to grow, or whether it saturates at the value for an ideal fluid.

A promising avenue to increase the energy density and/or increase the volume of high-density matter without any increase in beam energy is to collide heavy deformed (prolate) nuclei. This has been proposed by several theorists [10, 11, 12]. Central collisions with the long axes aligned with the beam (we call this the tip-to-tip configuration, as in Ref. [11]) would be the most desired configuration. However, as long as no beams of aligned deformed nuclei are available [13], the desired configurations have to be selected by experimenters using some

combination of triggering and online event selection. Recently, Heinz and Kuhlman advocated the use of full-overlap collisions between deformed uranium nuclei [12]. The selection of full-overlap collisions using Zero-Degree Calorimeters (ZDCs) was examined in Ref. [14]. However, various fluctuations and background signals in the detectors mean that an event sample with the lowest ZDC signal will still include a substantial fraction of collisions in which full overlap did not occur. In this work, we address these issues with the help of data on the relevant performance of the STAR detector [15].

The paper is organized as follows: in Sec. II we briefly review the relevant quantities and outline our calculation, while in Sec. III, we present results without and with detector smearing. In Sec. IV, we briefly summarize our findings.

II. BACKGROUND AND CALCULATIONAL FRAMEWORK

The elliptic flow anisotropy v_2 , defined as the second Fourier coefficient in the expansion

$$\frac{dN}{d\phi} = A [1 + 2v_n \cos(n\phi)] \quad (1)$$

of the azimuthal distribution $dN/d\phi$ of final state particles is a sensitive measure of the success of fluid-dynamical models. Based on suggestions in Refs. [16, 17, 18] it has become customary to consider $v_2 = \langle \cos(2\phi) \rangle$, the elliptic flow scaled by the initial spatial eccentricity [18]

$$v_2 = \frac{\langle y^2 \rangle - \langle x^2 \rangle}{\langle y^2 \rangle + \langle x^2 \rangle} \quad (2)$$

The normalization by $\langle y^2 \rangle + \langle x^2 \rangle$ emphasizes that the initial momentum anisotropy is driven by the initial geometry. One advantage of using $v_2 = \langle \cos(2\phi) \rangle$ is that the impact-parameter dependence is largely removed from its fluid-dynamically calculated value. This quantity is frequently plotted against the transverse particle density ($l = S$) dN_{ch}/dy , where dN_{ch}/dy is the multiplicity of charged particles

per unit rapidity and

$$S = \frac{p}{4\pi x^2 y^2} \quad (3)$$

is the transverse area of the overlap zone weighted by the number of wounded nucleons [5, 16, 19]. The transverse particle density $(1/S) dN_{ch}=dy$ can be interpreted as a measure of the initial entropy density in the transverse plane [12]. An increase in this quantity means increased particle production, and is thus associated with an increase in energy density in the system. The charged particle multiplicity per unit rapidity $dN_{ch}=dy$ can be increased by increasing the number of binary collisions, achievable by tip-to-tip collisions of heavy deformed nuclei. Furthermore, the U+U tip-to-tip configuration has about the same overlap area S as Au+Au collisions at $b = 0$, and thus contributes to a further increase in $(1/S) dN_{ch}=dy$ beyond what would be obtained with hypothetical spherical nuclei of the same mass as uranium. On the other hand, for $b = 0$ collisions, S increases by

24% between Au+Au and U+U when the latter are in the body-to-body orientation, i.e., when the long axes of the nuclei are parallel to each other, but perpendicular to the beam. Thus it can be concluded that even in the experimentally unrealistic limit where full-overlap U+U collisions can be isolated, it is necessary to also distinguish between different full-overlap configurations in order to realize the full potential advantage of U+U collisions.

The RHIC data as a function of $(1/S) dN_{ch}=dy$ reach the perfect-fluid value of $v_2 = 0.2$ in the most central 200 GeV Au+Au collisions at around $(1/S) dN_{ch}=dy \approx 28 \text{ fm}^{-2}$. Since viscosity would decrease the predicted v_2 , it would be difficult for a fluid-dynamical model to be reconciled with any further increase in the observed ratio v_2 . Thus, the behavior of this ratio at significantly larger $(1/S) dN_{ch}=dy$ should prove informative in assessing the applicability of fluid dynamics in central collisions at RHIC.

Uranium (^{238}U) beams have been proposed as a way to increase $(1/S) dN_{ch}=dy$ [10, 11, 12]. We assume in this study that, in order to isolate a sample of U+U collisions with the maximum possible $(1/S) dN_{ch}=dy$, the best available experimental procedure is to select events where the fewest possible spectator neutrons are detected (low ZDC signal) in coincidence with the highest observed multiplicity of produced particles in a broad region centered on mid-rapidity. Available data from the STAR experiment [15] describe this correlation and its fluctuation from event to event, and allow the output from the Monte-Carlo Glauber model described below to be filtered appropriately to simulate the relevant experimental limitations.

We represent the quadrupole deformation of the ground-state uranium nucleus in the standard [20] way: we take a Saxon-Woods density distribution with surface thickness $a = 0.535 \text{ fm}$ and with $R = R_{sp}(0.91 + 0.27 \cos^2 \theta)$, where θ is the polar angle relative to the symmetry axis of the nucleus and $R_{sp} = 1.12A^{1/3} = 0.86A^{1/3}$

fm [20]. The small hexadecapole moment of the uranium nucleus is neglected. This yields $R_{long} = R_{perp} \approx 1.29$ [9, 10, 12]. The orientation of the first and second nucleus in the colliding pair is fixed by the two angles (ϕ_p, ϕ_p) and (ϕ_t, ϕ_t) , respectively. The angles ϕ_p and ϕ_t describe the orientation of the symmetry axis relative to the beam direction, and they are uniformly distributed in $[0, \pi/2]$. The azimuthal angles ϕ_p and ϕ_t describe rotations about the beam direction, and they are uniformly distributed in $[0, 2\pi]$. A schematic view of a cut in the transverse plane illustrates the collision geometry in Fig. 1, where the lines represent equivalent sharp surfaces, and the shaded area corresponds to the overlap region in a collision at impact parameter b with fixed orientations of both nuclei. To simulate a uranium nucleus, 238 nucleons are selected

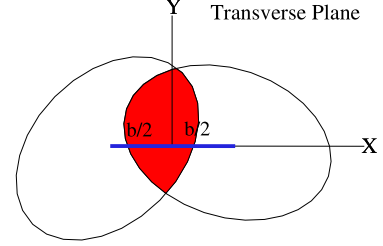


FIG. 1: Collision geometry.

randomly according to the appropriate Saxon-Woods distributions with distances between any two nucleons satisfying $r_{ij} \geq 0.4 \text{ fm}$. In the collision process, nucleons are considered wounded if the transverse distance between them becomes $\leq 4.2 \text{ fm}$, where we use 4.2 fm^2 for the nucleon-nucleon cross section at 200 GeV. To convert between track densities in rapidity y and in pseudorapidity η , we use the approximation $dN_{ch}=dy \approx 1.15 dN_{ch}=d\eta$ [21], and apply the parameterization

$$\frac{dN_{ch}}{d} = n_{pp} [xN_b + (1-x)N_w/2]; \quad (4)$$

where N_b is the numbers of binary collisions and N_w is the number of wounded nucleons [22]. The values of the parameters used are $x = 0.15$ and $n_{pp} = 2.19$ at 200 GeV. These values provide a reasonable fit to the PHOBOS data [23] as shown in Fig. 2.

III. RESULTS WITHOUT AND WITH DETECTOR SMEARING

A. No smearing

Figure 3 displays the charged multiplicity distribution $dN_{ch}=d$ for U+U collisions. Since we average over all possible orientations, this distribution is similar to that obtained for hypothetical spherical nuclei with mass 238. For ideal tip-to-tip U+U collisions ($b = 0 \text{ fm}$, $\phi_p = 0$, ϕ_t

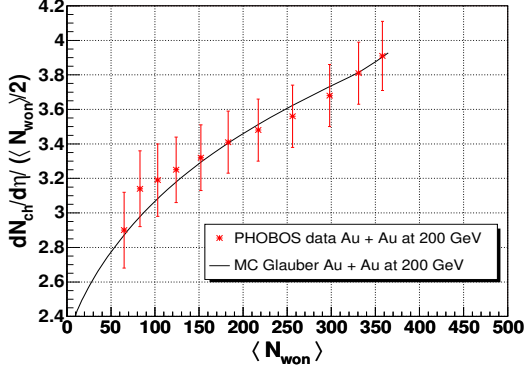


FIG. 2: Fit to PHOBOS data for Au+Au at 200 GeV, using Eq. (4).

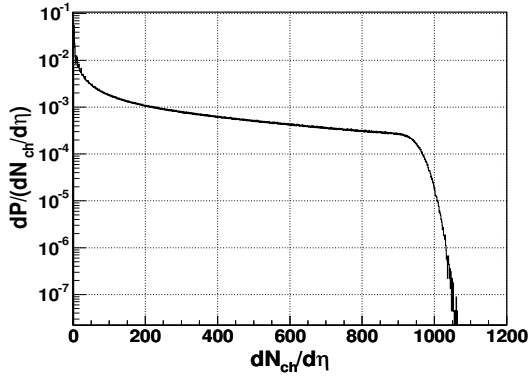


FIG. 3: Charged particle multiplicity distribution for U+U collisions.

$= 0$) we obtain $(1=S) dN_{ch}=dy \approx 42.6 \text{ fm}^2$. For body-to-body collisions ($b = 0$; $p = t = \infty$; $p = t = 0$) we have $(1=S) dN_{ch}=dy \approx 31.7 \text{ fm}^2$, surprisingly close to 31.5 fm^2 , the value for Au+Au at $b = 0 \text{ fm}$.

Although $dN_{ch}=dy$ is larger for U+U than for Au+Au, the larger overlap area for body-to-body collisions offsets the increase and results in a value of $(1=S) dN_{ch}=dy$ close to that for Au+Au. The approximately 35% increase in $(1=S) dN_{ch}=dy$ in tip-to-tip U+U collisions compared to Au+Au is due to the increase in $dN_{ch}=dy$, since the overlap areas are similar in these cases.

Under the best of circumstances, an experiment can hope to select certain ranges of angles and impact parameter. For illustrative purposes, we choose a somewhat arbitrary range of definitions for near tip-to-tip collisions: $b \leq 1$ or 2 fm , with p and t both within 10° or 20° , and for simplicity we keep $p = t$ throughout.

Even if we impose the strictest definition above for near tip-to-tip events ($p = t \leq 10^\circ$ and $b \leq 1 \text{ fm}$) and a similarly restrictive definition for near body-to-body collisions, almost all of the near tip-to-tip and near body-to-body events lie in the top 3% of the $dN_{ch}=d$ (or, equivalently $dN_{ch}=dy$) distribution. For Au+Au col-

lisions with $dN_{ch}=dy$ in the top 3% of the event sample, the additional requirement that the number of spectator nucleons lie in the bottom 1% of its parent distribution leads to little or no further change in $(1=S) dN_{ch}=dy$. For near tip-to-tip U+U configurations, there are significant increases of 32{36% over central Au+Au. Details related to various near tip-to-tip U+U selection conditions can be found in Table I, and as before, a spectator cut has negligible additional effect on $(1=S) dN_{ch}=dy$. If a near body-to-body configuration is defined as $0 \leq b \leq 1 \text{ fm}$, $p, t \leq 80^\circ$, and $j_p = j_t \leq 10^\circ$, then the mean value of $(1=S) dN_{ch}=dy$ comes out to be 31.3 fm^2 , very close to the ideal body-to-body case mentioned above, and still negligibly different from the value for central Au+Au.

	spectator count	$0 \leq b \leq 1 \text{ fm}$ % evt	$h_S^{-1} \frac{dN_{ch}}{dy} _{i=1}$	$0 \leq b \leq 2 \text{ fm}$ % evt	$h_S^{-1} \frac{dN_{ch}}{dy} _{i=1}$
10	any	0.174	42.25	0.687	41.59
20	any	0.707	41.75	2.756	41.13
10	lowest 1%	0.173	42.26	0.478	41.95
20	lowest 1%	0.704	41.76	1.903	41.50

TABLE I: Mean values of $(1=S) dN_{ch}=dy$ and percentage of the event class in near tip-to-tip U+U configurations relative to the number of events in the top 3% of $dN_{ch}=dy$.

In the discussion above, central collisions were selected primarily via their high multiplicity. Next, we use a low spectator count as the initial centrality criterion, and explore the effect of an additional cut on total multiplicity. Results are presented in Fig. 4, and it is evident that the ratio of near tip-to-tip to near body-to-body events increases very substantially as more central collisions are selected. However, even for the 5% of collisions with highest multiplicity, the near tip-to-tip category remains only about 21% of the events with a low spectator count (the latter being defined as the lowest 1% of all collisions, regardless of multiplicity).

B. With smearing

In the previous section, we defined ranges of U+U collision configurations termed "near tip-to-tip" and "near body-to-body". These ranges were defined for illustrative purposes only; in this section, we estimate the characteristics of a class of events intended to have the highest experimentally obtainable enrichment of the desired tip-to-tip configurations. We assume that this is carried out by selecting events with the highest charged particle multiplicity in a broad region centered on midrapidity, and simultaneously cutting to select events with a low signal in both Zero Degree Calorimeters.

The measured $dN_{ch}=d$ in a detector like STAR is linearly correlated with the true $dN_{ch}=d$, but is subject to random event-to-event fluctuations in the efficiency for detecting tracks as well as random variations in the inclusion rate for tracks that do not originate from the

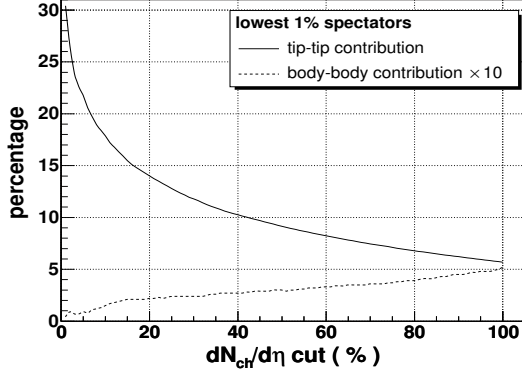


FIG. 4: Among events where the spectator nucleon count lies in the lowest 1% of all collisions, the percentage of near tip-to-tip ($\tau = 20$; $b = 2$ fm) and near body-to-body ($\tau = 70$; $j_p = j_p = 20$, $b = 2$ fm) configurations as a function of an additional cut on $dN_{ch}/d\eta$. The horizontal scale is normalized such that 100% corresponds to the full sample where only the spectator cut has been applied.

primary collision vertex. Similarly, the ZDC signals have a component that is proportional to the number of emitted spectator neutrons as well as a component from various sources of background. Furthermore, the RHIC intersection regions are arranged such that the ZDCs have acceptance for only free neutrons and an insignificantly small fraction of neutron-rich charged spectator fragments. Thus while we compute the total number of spectator nucleons in a given event using our Monte Carlo Glauber model, in real collisions at STAR, only a subset of the spectators are detected by the ZDCs, and so events with a small ZDC signal include a high background level of collisions with incomplete overlap.

The upper panel of Fig. 5 shows contours of event density in the plane of spectator count versus $dN_{ch}/d\eta$ from our Monte Carlo Glauber model without any detector simulation. The resulting correlation is much narrower than what is observed in experiment [15], an expected outcome given the simplicity of the model and the neglect of the experimental effects discussed above. To make a realistic estimate of the best enrichment of tip-to-tip U+U collisions that might be achieved, it is necessary to smear out the narrow ridge in the upper panel of Fig. 5 so that a pattern resembling the experimental distribution is obtained. For this purpose, a Gaussian-distributed random number is first added to $dN_{ch}/d\eta$ for each event, such that the steeply dropping upper tail of the $dN_{ch}/d\eta$ distribution in Fig. 3 is smeared out to the point where it resembles the experimental distribution from STAR. The smeared multiplicity distribution is shown in Fig. 6. Note that we are concerned here with the upper end of the multiplicity distribution (highest values of $dN_{ch}/d\eta$), and the variation of the smearing at lower multiplicities is not of interest.

Next, another Gaussian-distributed random number (with non-zero mean) is added to the spectator count

and the result is used as the simulated ZDC signal. The Gaussian mean and width are adjusted to produce a ridge near the lower right part of the lower panel of Fig. 5 that resembles the observed data from STAR [15]. This procedure has a small effect on the agreement of the calculation with the PHOBOS data shown in Fig. 2, and while the effect is minimal, we corrected for the difference.

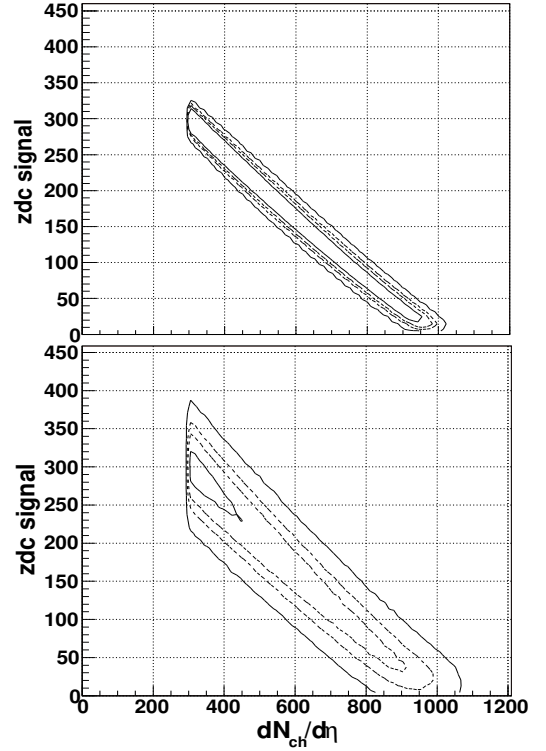


FIG. 5: Contours of event density in the plane of simulated ZDC signal versus $dN_{ch}/d\eta$ before (upper panel) and after (lower panel) simulation of detector-related smearing and background. The contour levels are the same in both panels, with a ratio of 1:7 between the two outermost contours, and a ratio of 1:2 between all other adjacent contours.

Various combinations of cuts in $dN_{ch}/d\eta$ and in ZDC signal have been applied to the simulated U+U data plotted in the lower panel of Fig. 5 with the objective of maximizing the transverse particle density $(1/S) dN_{ch}/d\eta$. Because the quantity we seek to maximize is trivially correlated with one of our cut variables, we assess the maximum particle density in U+U collisions relative to Au+Au collisions with the same cuts on a percentage basis.

The vertical axis in Fig. 7 shows the ratio $[(1/S) dN_{ch}/d\eta]_{U+U} / [(1/S) dN_{ch}/d\eta]_{Au+Au}$ as a function of independent scans across both cut variables. Note the zero-suppressed vertical axis; we conclude that no further increase in $[(1/S) dN_{ch}/d\eta]_{U+U}$ beyond about 18% relative to Au+Au can be reached in the context of our simulation, even searching beyond the plotted combina-

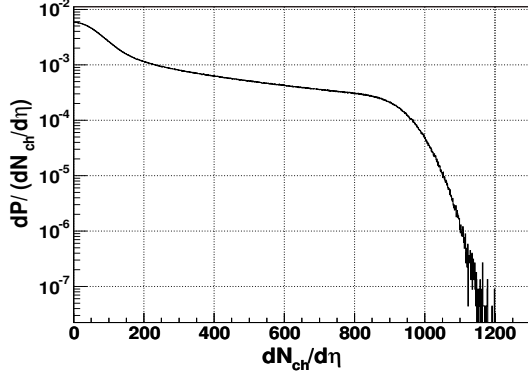


FIG. 6: Charged particle multiplicity distribution in U+U collisions after detector smearing.

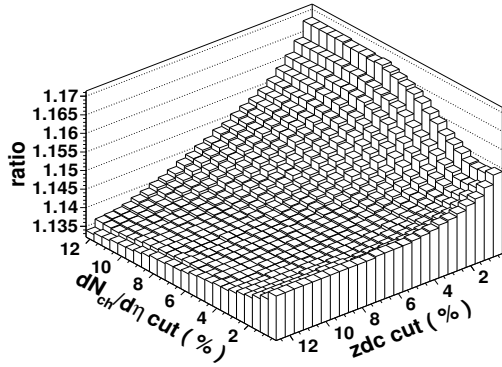


FIG. 7: Ratio $[(1=S)dN_{ch}=dy]_{U+U} / [(1=S)dN_{ch}=dy]_{Au+Au}$ as a function of different $dN_{ch}=d$ and ZDC cuts, labeled according to the selected percentage of the total sample.

tions of cuts on $dN_{ch}=d$ and ZDC signal. In the region of the most selective combination of centrality cuts, the advantage of U+U is about 16%.

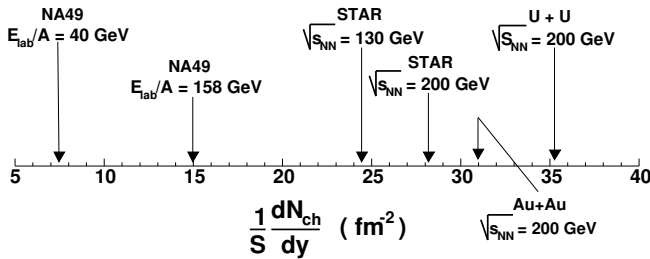


FIG. 8: Maximum values of $(1=S)dN_{ch}=dy$. Values from NA49 and STAR correspond to central Pb+Pb [19] and central Au+Au [5], respectively. The results labeled Au+Au $\sqrt{s_{NN}} = 200$ GeV and U+U $\sqrt{s_{NN}} = 200$ GeV correspond to the top 5% in $dN_{ch}=d$ from the present simulation.

Figure 8 summarizes the measured progression in the

maximum $(1=S)dN_{ch}=dy$ for central Pb+Pb or Au+Au collisions, beginning with a low SPS beam energy and continuing to the highest RHIC energy. On the same number line, we indicate that when our simulation for Au+Au is constrained to agree well with the value from the STAR collaboration, we predict a potential further increase of about 4 fm^2 for U+U with the same centrality cut.

IV. CONCLUSION

We have undertaken a study of the potential for U+U collisions to realize an increased transverse particle density $(1=S)dN_{ch}=dy$ without increasing the beam energy. We note that the present investigation addresses only a limited aspect of U+U collisions, namely, we have studied the "worst case scenario" where only the transverse particle density $(1=S)dN_{ch}=dy$ is of interest, and where the charged particle multiplicity and the Zero-Degree Calorimeter signals are the only means of selecting the desired U+U events. Previous studies have considered the issue of the path-dependent energy loss of partons in the unique participant geometry of central U+U collisions [10, 12], and it is feasible for U+U collisions to extend our physics reach in a variety of observables.

The transverse particle density increases by about 35% in the ideal limit of tip-to-tip U+U collisions compared to Au+Au at zero impact parameter. However, the practical limitation of selecting the U+U samples of interest via conventional measures of centrality, as used in RHIC experiments, leads to uranium beams offering a smaller, yet still worthwhile advantage. Specifically, our simulations suggest that the maximum achievable values of $(1=S)dN_{ch}=dy$ at RHIC could be increased from the present 31 fm^2 to about 35 fm^2 with U+U collisions. This increase should justify the needed investment of effort and resources at RHIC, being of the same order as the measured increase for central Au+Au collisions when the beam energy was increased from $\sqrt{s_{NN}} = 130$ GeV to 200 GeV, or just under half the increase between the top CERN SPS energy and $\sqrt{s_{NN}} = 130$ GeV.

V. ACKNOWLEDGMENTS

We thank Ulrich Heinz, Anthony Kuhlman, and Peter Levai for extensive discussions. One of the authors (GF) acknowledges the support of a Szent-Gyorgyi Scholarship of the Hungarian Department of Education and the hospitality of the Eotvos University, where some of this work was carried out. This work was supported in part by US DOE grants DE-FG 02-86ER 40251 and DE-FG 02-89ER 40531.

-
- [1] M. Gyulassy and L. McLerran, Nucl. Phys. A 750, 30 (2005) [[arXiv:nucl-th/0405013](#)].
 - [2] I. Arsene et al. [BRAHMS Collaboration], Nucl. Phys. A 757, 1 (2005) [[arXiv:nucl-ex/0410020](#)].
 - [3] K. Adcox et al. [PHENIX Collaboration], Nucl. Phys. A 757, 184 (2005) [[arXiv:nucl-ex/0410003](#)].
 - [4] B. B. Back et al., Nucl. Phys. A 757, 28 (2005) [[arXiv:nucl-ex/0410022](#)].
 - [5] J. Adams et al. [STAR Collaboration], Nucl. Phys. A 757, 102 (2005) [[arXiv:nucl-ex/0501009](#)].
 - [6] F. Karsch, Prog. Theor. Phys. Suppl. 153, 106 (2004) [[arXiv:hep-lat/0401031](#)].
 - [7] T. Hirano and M. Gyulassy, [arXiv:nucl-th/0506049](#).
 - [8] http://www.bnl.gov/bnlweb/pubaf/pr/PR_display.asp?prID=05-38.
 - [9] P. F. Kolb, J. Sollfrank and U. W. Heinz, Phys. Rev. C 62, 054909 (2000) [[arXiv:hep-ph/0006129](#)].
 - [10] E. V. Shuryak, Phys. Rev. C 61, 034905 (2000) [[arXiv:nucl-th/9906062](#)].
 - [11] B. A. Li, Phys. Rev. C 61, 021903 (2000) [[arXiv:nucl-th/9910030](#)].
 - [12] U. W. Heinz and A. Kuhlman, Phys. Rev. Lett. 94, 132301 (2005).
 - [13] D. Fick, J. Phys. (Paris) Colloq. C 6, 265 (1990).
 - [14] A. J. Kuhlman and U. W. Heinz, Phys. Rev. C 72, 037901 (2005) [[arXiv:nucl-th/0506088](#)].
 - [15] K. H. Ackermann et al. [STAR Collaboration], Nucl. Instrum. Meth. A 499, 624 (2003); F. S. Bieser et al., Nucl. Instrum. Meth. A 499, 766 (2003); C. Adler, A. Denisov, E. Garcia, M. Murray, H. Strobele and S. White, Nucl. Instrum. Meth. A 499, 433 (2003).
 - [16] H. Heiselberg and A. M. Levy, Phys. Rev. C 59, 2716 (1999) [[arXiv:nucl-th/9812034](#)].
 - [17] H. Sorge, Phys. Rev. Lett. 82, 2048 (1999) [[arXiv:nucl-th/9812057](#)].
 - [18] S. A. Voloshin and A. M. Poskanzer, Phys. Lett. B 474, 27 (2000) [[arXiv:nucl-th/9906075](#)].
 - [19] C. Alt et al. [NA 49 Collaboration], Phys. Rev. C 68, 034903 (2003) [[arXiv:nucl-ex/0303001](#)].
 - [20] A. Bohr and B. R. Motelson, Nuclear Structure (Benjamin, New York, 1969), Vol. II.
 - [21] C. Adler et al. [STAR Collaboration], Phys. Rev. C 66, 034904 (2002) [[arXiv:nucl-ex/0206001](#)].
 - [22] D. Kharzeev and M. Nardi, Phys. Lett. B 507, 121 (2001) [[arXiv:nucl-th/0012025](#)].
 - [23] B. B. Back et al. [PHOBOS Collaboration], Phys. Rev. C 65, 061901 (2002) [[arXiv:nucl-ex/0201005](#)].